Electronic Supplementary Material (ESI) for Chemical Science.

Supplementary Information

Orbital Electron Delocalization of Axial-coordinated Modified FeN_4 and Structurally Ordered PtFe Intermetallic Synergistically for Efficient Oxygen Reduction Reaction Catalysis

Chenzhong Wu, Meida Chen, Bin Wang, Leqing Luo, Qian Zhou, Guangtao Mao, Yuan Xiong and Qingmei Wang*

Guizhou University Key Laboratory of Green Chemical and Clean Energy Technology, Guizhou University Engineering Research Center of Efficient Utilization for Industrial Waste, Institute of Dual-carbon and New Energy Technology Innovation and Development of Guizhou Province, School of Chemistry and Chemical Engineering, Guizhou University, Guiyang 550025, China. E-mail: qmwang3@gzu.edu.cn (Q. M. Wang)

Table of Contents:

Experimental and Computational Section

Chemicals and Materials

Hemin ($C_{34}H_{32}ClN_4O_4Fe$, ≥95%), Methanol (CH_3OH), Platinum Dichloride ($PtCl_2$, Pt basis ≥73%), Hydrochloric Acid (HCl) and Nitric Acid (HNO_3) were purchased from Macklin. Deionized (DI) water from Milli-Q System (Millipore, Billerica, MA) was used in all our experiments. 5wt % Nafion solution was purchased from Aldrich. The commercial Pt/C catalyst (JM, 20wt% Pt loading) was procured from Sunlaite. The 20wt% Pt/C catalyst is ~3 nm Pt nanoparticles loaded on Vulcan XC-72 carbon support. All the chemicals were used as purchased without any further purification.

Synthesis of Pt_1Fe/FeN_4CCl, Pt_2Fe/FeN_4CCl, and Pt_3Fe/FeN_4CCl catalysts

The 0.092 mmol, 0.170 mmol, and 0.276 mmol hemin were respectively added into the contained 20 mL methanol beaker. Immediately, the above mixture solution was uniformly dispersed by stirring ultrasonically for 0.5 h. The 2100 uL Platinum dichloride was added to the above solutions ultrasonically for 0.5 h and stirred for 12 h. The evenly dispersed solution was transferred to an oven and dried at 60 °C to obtain the Pt-Fe-N-C-Cl precursor, then centrifugation (9000 rpm/s) and washed. Next, the dried Pt-Fe-N-C-Cl precursor was heated to 800 °C high temperature for 2 h with a heating rate of 5 °C·min^{-1} in a flowing atmosphere (95% N_2 /5% H_2), and then naturally cooled to room temperature. Subsequently, the cooled composite materials were washed with 1 mol/L HNO_3 to remove metallic impurities at room temperature. Finally, the Pt_2Fe/FeN_4CCl was obtained after centrifugation, washed and drying. Furthermore, the Pt_1Fe/FeN_4CCl and Pt_3Fe/FeN_4CCl sample was equally prepared by pyrolysis at 800 °C changing only the content of hemin. The electrochemical measurements of all as-prepared catalysts were directly utilized without further post-treatment.

Characterization

The crystal structure and properties of the synthetic materials were studied using powder XRD on a D8 advance diffractometer (Bruker AXS, Germany) with Cu source (λ = 1.5406 Å), equipped with a position-sensitive detector in the angular range $0^o \leq 2\theta \leq 90^o$ with a step rate of 5º min^{-1}. To collect the lattice shrinkage and strain variety data, the Debye–Scherrer equation is used to calculate, and the specific calculation equations are as follows:

$$N=1/2d \quad (1)$$

$$N_2\ strain\%=(N_1-N_2)/N_1 \quad (2)$$

N and d refer to the lattice parameters and lattice spacing, respectively (Take the (111) crystal plane as the calculation plane). N_1 and N_2 strain% represent the lattice parameter (Pt/C) and the percentage of lattice parameter variation (Pt_1Fe/FeN_4CCl, Pt_2Fe/FeN_4CCl, and Pt_3Fe/FeN_4CCl relative to Pt/C), respectively.

The TEM images, HAADF-STEM, and energy-dispersive spectroscopy (EDS) were obtained by a JEM ARM200F equipped with a cold field-emission gun and aberration corrector microscope at 200 kV acceleration voltage. The nanoparticle sizes were measured with Nano measurer 1.2 software, and the total number of particles in this

statistic is 100. The XPS analysis was carried out using a Kratos AXIS Ultra DLD XPS (Kratos Analytical). The XPS system is equipped with a monochromatic Al Kα source operated at 15 keV and 150 W, a hemispherical analyzer, a charge neutralizer, a catalysis cell, and a load lock chamber for the rapid introduction of samples without breaking the vacuum. X-rays were incident at an angle of 45° with respect to the surface normal. Analysis was performed at a pressure of $\sim 1 \times 10^{-9}$ mbar and high-resolution core level spectra were measured with a pass energy of 40 eV. The XPS experiments were performed using an electron beam, directed to the sample, for charge neutralization. In-situ reduction of the materials was performed in a reaction cell (Model: ES-009R01) directly attached to the XPS chamber, which allows the sample to be treated under gas flow conditions. The samples were transferred inside the reaction cell and back to the analysis chamber without exposure to the atmosphere. All the peaks were adjusted using the C 1s peak at 284.8 eV as the reference. The ICP-OES analysis was manipulated on an Elan DRC-e instrument.

XANES and EXAFS experiments at 300 K were performed at PETRA III, beamline P64, of DESY, Germany. Measurements of Pt L_3-edges and Fe K-edge at ambient pressure were performed in fluorescence as well as transmission mode using gas ionization chambers to monitor the incident and transmitted X-ray intensities. Monochromatic X-rays were obtained using a Si (111) double crystal monochromator which was calibrated by defining the inflection point (first derivative maxima) of Cu foil as 8980.5 eV. The beam was focused by employing a Kirkpatrick-Baez (K-B) mirror optic. A rhodium-coated X-ray mirror was used to suppress higher-order harmonics. A CCD detector was used to record the transmitted signals. Pellets for the ex-situ measurements were made by homogeneously mixing the sample with an inert cellulose matrix to obtain an X-ray absorption edge jump close to one.

Pt foil, PtO_2, Fe foil, FeO, and FePc were used as standard samples to evaluate the coordination environment and chemical state of Pt L_3-edge and Fe K-edge of Pt_2Fe/FeN_4CCl samples. According to the energy correction of Pt foil and Fe foil, the signals of Pt L_3-edge and Fe K-edge were optimized using the ATHENA program in the IFEFFIT software package,[1] and then alignment of the EXAFS data (E_0) was determined based on the highest value of the first derivative of XANES. Through the corrected XANES white line peak position, the chemical valence range of Pt and Fe in the as-prepared Pt_2Fe/FeN_4CCl catalyst could be determined. For EXAFS analysis, the Pt L_3-edge and Fe K-edge of k space range (2.0-12.0 $Å^{-1}$) was selected for Fourier transform (FT) to obtain R space, where the k-weight was 2. The first shell of R space was selected for inverse Fourier transform to obtain q space, involving Pt L_3-edge of Pt foil (1.0-3.0 Å), PtO_2 (1.0-3.0 Å) and Pt_2Fe/FeN_4CCl (1.0-3.0 Å), as well as Fe K-edge of Fe foil (1.0-3.0 Å), FeO (1.0-3.0 Å), Pt_2Fe/FeN_4CCl (1.0-3.0 Å) and FePC (1.0-3.0 Å). The subsequent theoretical EXAFS models were constructed and fitted to the experimental data in ARTEMIS, involving Pt L_3-edge of Pt foil (1.25-3.0 Å), PtO_2 (1.0-3.0 Å) and Pt_2Fe/FeN_4CCl (1.25-2.8 Å), as well as Fe K-edge of Fe foil (1.0-3.0 Å), FeO (1.0-3.0 Å), Pt_2Fe/FeN_4CCl (1.0-3.0 Å) and FePc (1.0-3.0 Å) and the value range of k and R space was the same as the selection in the abovementioned FT and inverse Fourier transform. According to the set coordination number of Pt foil (12) and Fe

foil (6 and 8), the amplitude reduction factor $S0^2$ of Pt L_3-edge and Fe K-edge was obtained by fitting the ARTEMIS program. After EXAFS fitting, the detailed fitting information of Pt_2Fe/FeN_4CCl could be recorded, including the coordination number, bonding length, Debye-Waller factor, and energy shift, etc. More EXAFS fitting information is shown in Supplementary Information Table S3 and Table S4.

Electrochemical Measurements

Electrochemical analysis was performed in a standard three-electrode system by applying an electrochemical workstation (Donghua test, Dh7003). The standard three-electrode is formed of a working electrode (glassy carbon (GC)), reference electrode (Ag/AgCl), and counter electrode (carbon rod). All potential, unless mentioned otherwise, were transformed to the reversible hydrogen electrode (RHE). To manufacture the catalyst ink, 2 mg of all as-prepared catalyst was dissolved in the mixed solutions, which contained ethanol (790uL) and Nafion solutions (10 uL), and then ultrasonicated for 0.5 h. Immediately, the 8 uL ink of all as-prepared catalysts was measured by utilizing a pipette and drop-dried onto a working electrode to obtain ~2 ug Pt loading (the area of 0.19625 cm^2). The commercial Pt/C catalyst as reference was pursued to similarly process operation. Subsequently, the 8 uL ink of commercial Pt/C catalyst was drop-dried onto a working electrode to obtain ~4 ug Pt loading. The cyclic voltammetry (CV) is carried out by applying cyclic scans between 0.05 to 1.2 V (vs RHE) in fresh N_2-saturated 0.1 M $HClO_4$ electrolyte solutions (sweep rate: 0.05V/s). The oxygen reduction reaction (ORR) analysis is implemented in O_2-saturated 0.1 M $HClO_4$ electrolyte solutions (sweep rate: 0.01V/s; rotating speeds: 1600 rpm). The CO stripping experiments are operated in 0.1M $HClO_4$ electrolyte solutions. The CO gas is bubbled into electrolyte solutions for ~20 min. Then the dissolved CO is purified using high-purity N_2-saturated for 0.5h in the 0.1 M $HClO_4$ electrolyte solutions. The accelerated durability test (ADT) is executed in O_2-saturated 0.1 M $HClO_4$ solutions, and a cyclic potential scan of 40,000 CV cycles is performed at a scanning rate of 50 mV/s between 0.6 and 1.2 V. The cyclic potential scan of commercial Pt/C catalyst was only circulated 30,000 CV cycles at a scanning rate of 50 mV/s between 0.6 and 1.2 V.

According to the peak area of CO stripping and the loading of Pt on the electrode, we calculate the electrochemical surface area (ECSA) of the catalysts via the following equation:

$$ECSA_{CO}=Q_{CO}/(0.42*[Pt]) \quad (1)$$

Q_{CO} refers to the electric quantity calculated by the integral of CO stripping peak. The [Pt] refers to the loading quantity of Pt on the electrode (mg/cm^2).

The electron transfer number (n) was gained from the ORR polarization curves tested with different rotating speeds from 625 to 2500 rpm, using Koutecky-Levich first order:

$$j^{-1}=j_K^{-1}+j_L^{-1}=j_L^{-1}+B^{-1}\omega^{-1/2} \quad (2)$$

where $B = 0.2nFD_0^{2/3}C_0v^{-1/6}$. In eq (2), j is the measured current density, which

consists of kinetic (j_K) and diffusion-limiting current (j_L); B is a constant; ω is the rotation speed in rpm; F is the Faraday constant (96485 C/mol); n is the number of electrons transferred per oxygen molecule; C_0 is the bulk concentration of O_2 (1.5×10^{-3} mol/L in 0.1 M $HClO_4$); D_0 is the diffusion coefficient for O_2 in 0.1 M $HClO_4$ (2.0×10^{-5} cm^2/s); and v is the kinetic viscosity of the solution (0.01 cm^2/s). A constant of 0.2 was used for B when the unit of rotation speed is given in rpm.

DFT computational details

All spin-polarization periodic density functional theory (DFT) calculations were performed within the frame of Vienna ab initio simulation package (VASP).[2] The projector augmented wave (PAW) method was used to describe the ionic cores.[3] And the generalized gradient approximation (GGA) with the Perdew-Burke-Ernzerhof (PBE) exchange-correlation functional were employed to model the electron exchange-correlation.[4] A cutoff energy of 450 eV is utilized for the plane wave basis set. The equilibrium geometries were obtained when the maximum atomic forces are smaller than 0.02 eV/Å and by employing a total energy convergence of 10^{-5} eV for the electronic self-consistent field loop. ORR calculations were performed on two different sets of models: (a) PtFe where a five layers 2*2 structure was utilized with 5*5 *1 k-point grid, and (b) structures for the FeN_4C, FeN_4CCl, PtFe/FeN_4CCl and PtFe cluster with 2*3*1 k-point grid. 6*8*1 k-point grid was used for density of states calculation of FeN_4C and FeN_4CCl systems. All models have 15 Å vacuum layer along the z-direction. The bottom two atomic layers of PtFe were fixed, while other atoms were relaxed during all the calculations.

The ORR process contains following steps:

$$* + O_2 + H_2O \rightarrow *OOH + OH^- - e^- \quad (1)$$

$$*OOH \rightarrow *O + OH^- - e^- \quad (2)$$

$$*O + H_2O \rightarrow *OH + OH^- - e^- \quad (3)$$

$$*OH \rightarrow * + OH^- - e^- \quad (4)$$

The adsorption free energy of ORR intermediates was calculated using the equations:

$$\Delta G_{*OOH} = G_{*OOH} + \frac{3}{2}G_{H_2} - G_* - 2G_{*H_2O} \quad (a)$$

$$\Delta G_{*O} = G_{*O} + G_{H_2} - G_* - G_{*H_2O} \quad (b)$$

$$\Delta G_{*OH} = G_{*OH} + \frac{1}{2}G_{H_2} - G_* - G_{*H_2O} \quad (c)$$

The Gibbs free energy G of each species was calculated as follow:

$$G = E + ZPE - TS \quad (5)$$

where G, E, ZPE and TS are the free energy, total energy from DFT calculations, zero-point energy and entropic contributions (T was set to be 300K), respectively. ZPE and TS could be derived after frequency calculation.

Supplementary Schemes

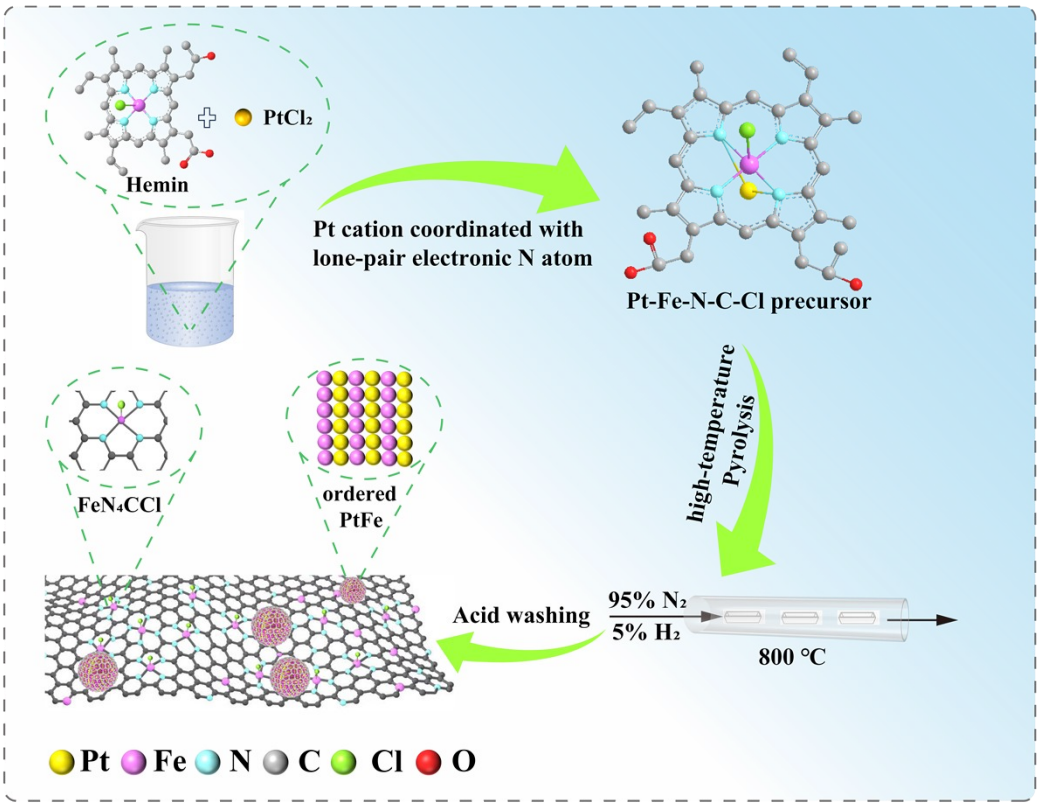

Scheme S1 Schematic illustration of the main steps for fabricating structurally ordered Pt_xFe/FeN_4CCl catalysts, where X represents the weight ratio of contained Pt to Fe in the precursor (X = 1, 2, and 3, respectively. Firstly, the Pt-Fe-N-C-Cl precursor was afforded in low-temperature environment incubation, in which the adsorption process was grounded on the platinum-nitrogen coordination complexation between lone-pair electronic N atom in the hemin-Cl and platinum cation. Subsequently, Pt-Fe-N-C-Cl precursor, derived from the hemin, could generate as-prepared Pt_xFe/FeN_4CCl catalysts integrated structurally ordered PtFe intermetallic with the FeN_4CCl substrate by an in-situ pyrolysis of reduction strategy. A partial Fe atom in the precursor hemin-Cl alloying with Pt atoms and forming axial chlorine-coordinated modified Fe single-atom with other ones.

Supplementary Figures

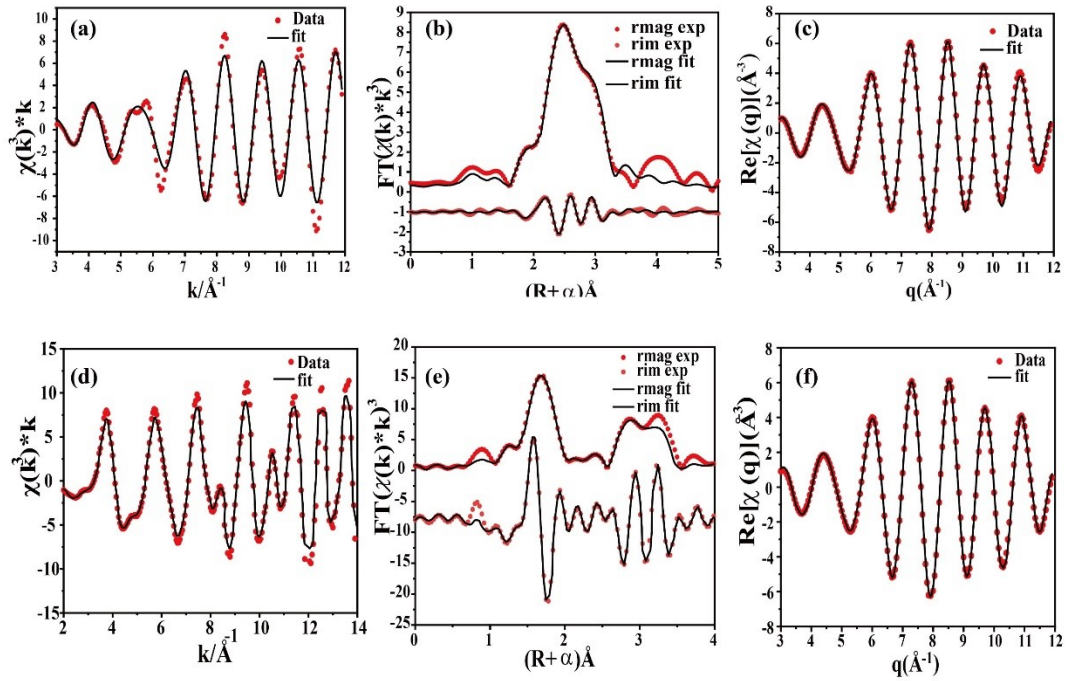

Figure S1 Pt L_3-edge EXAFS (points) and curve-fit(line) for (a)Pt foil; (d) PtO_2 shown in k^2-weighted k-space. Pt L_3-edge EXAFS (points) curve-fit (line) for (b) Pt foil; (e) PtO_2 shown in R-space (FT magnitude and imaginary component. The data are k^2-weighted and not phase-corrected). Pt L_3-edge EXAFS (points) curve-fit (line) for (c) Pt foil; (f) PtO_2 shown in k^2-weighted in inverse FT-EXAFS.

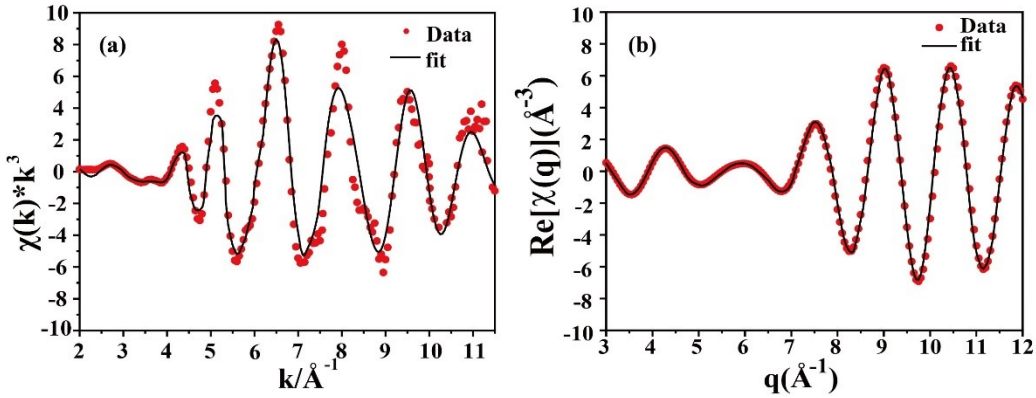

Figure S2 (a-b) shown Pt L_3-edge EXAFS (points) and curve-fit(line) for Pt_2Fe/FeN_4CCl in k^2-weighted k-space (a) and inverse FT-EXAFS (b).

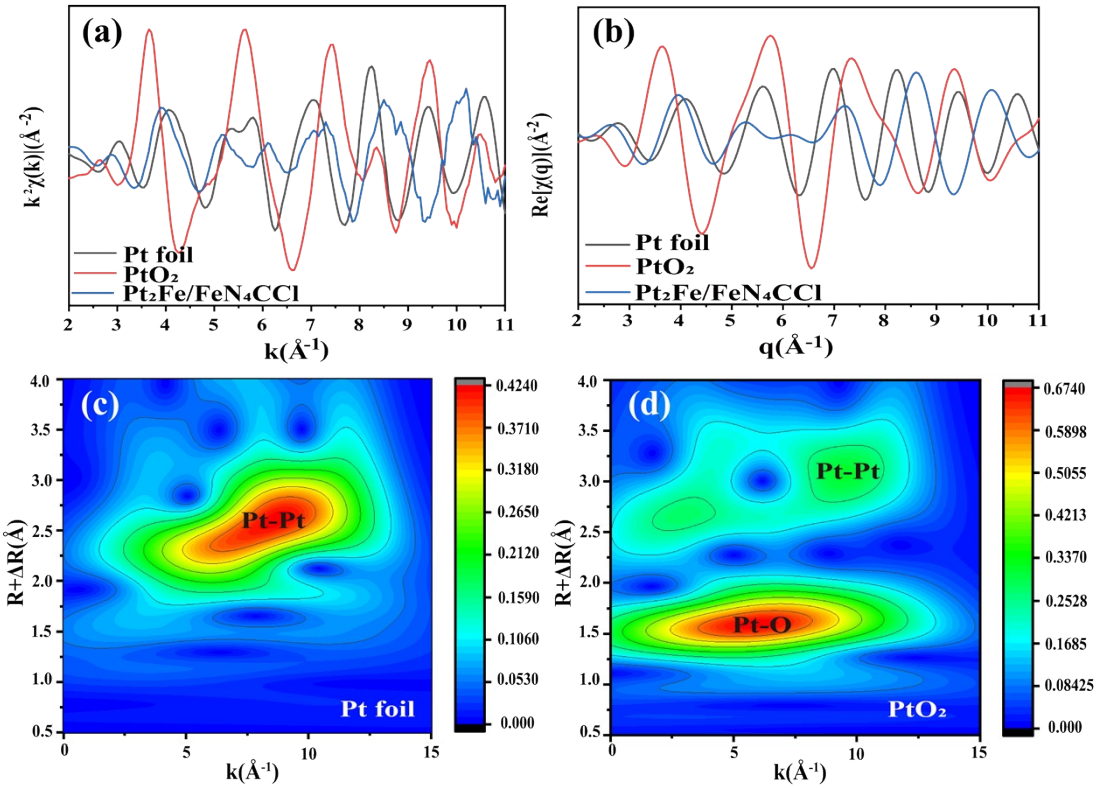

Figure S3 The data results curve of Pt L_3-edge EXAFS shown k space (a) and inverse FT-EXAFS (b) for Pt foil, PtO_2 and Pt_2Fe/FeN_4CCl. The diagram of Wavelet transforms analysis of the Pt L_3-edge of corresponding EXAFS spectra for Pt foil (c) and PtO_2 (d).

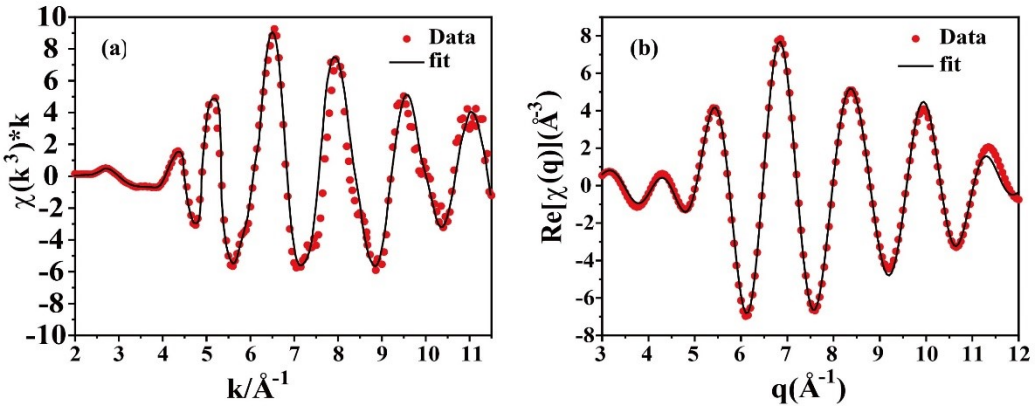

Figure S4 (a-b) shown Fe K-edge EXAFS (points) and curve-fit(line) for Pt_2Fe/FeN_4CCl in k^2-weighted k-space (a) and inverse FT-EXAFS (b).

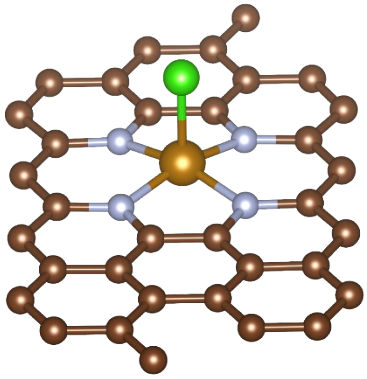

Figure S5 The three-dimensional moiety shows the schematic model of FeN_4Cl: Fe (gold), N (gray), Cl (green), and C (brown).

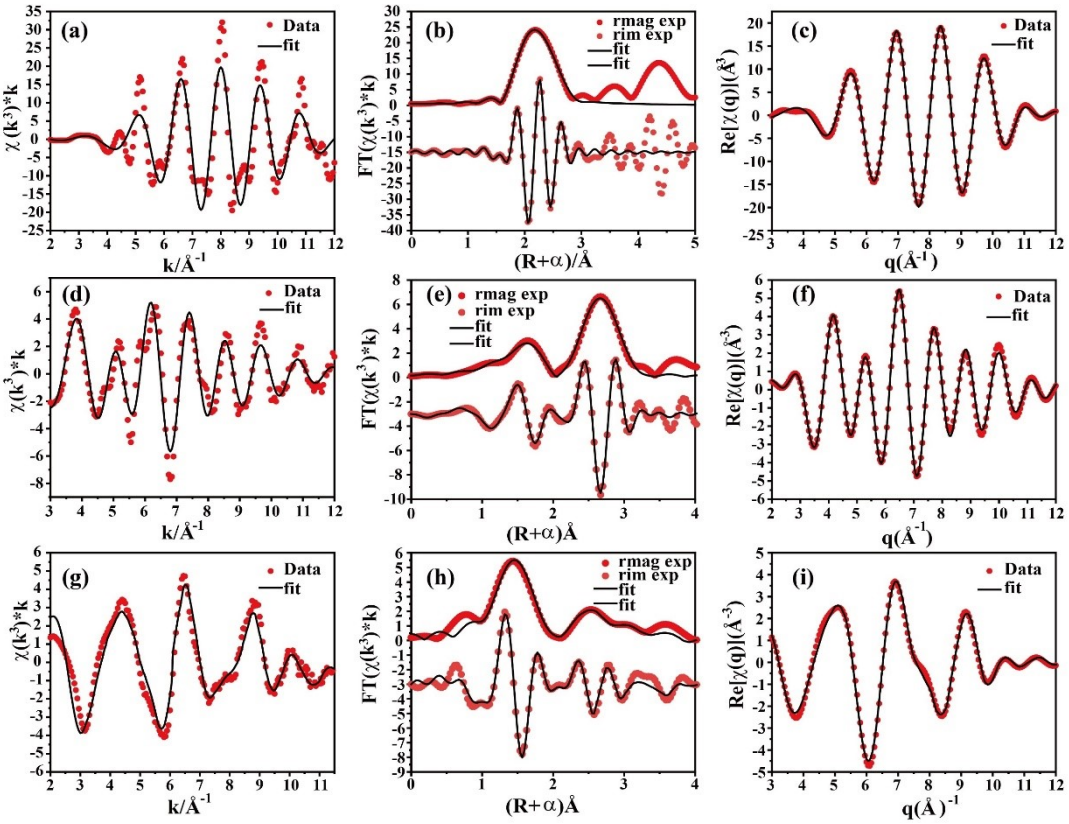

Figure S6 Fe K-edge EXAFS (points) and curve-fit(line) for (a)Fe foil, (d)FeO and (g)FePc shown in k^2-weighted k-space. Fe K-edge EXAFS (points) and curve-fit (line) for (b)Fe foil, (e)FeO and (h) FePc shown in R-space (FT magnitude and imaginary component. The data are k^2-weighted and not phase-corrected). Fe K-edge EXAFS (points) and curve-fit (line) for (c)Fe foil, (f) FeO and (i)FePc shown in k^2-weighted in inverse FT-EXAFS.

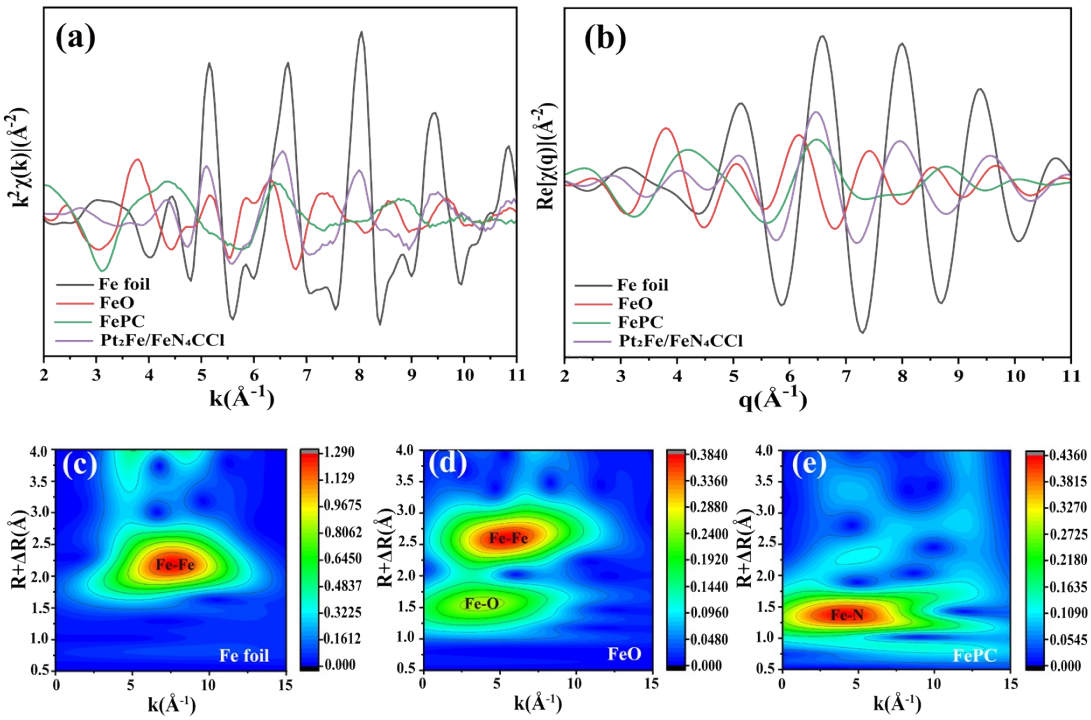

Figure S7 The data results curve of Fe K-edge EXAFS shown k space (a) and inverse FT-EXAFS (b) for Fe foil, FeO, FePc and Pt_2Fe/FeN_4CCl. The diagram of Wavelet transforms analysis of the Fe K-edge of corresponding EXAFS spectra for Fe foil (c), FeO (d) and FePc (e).

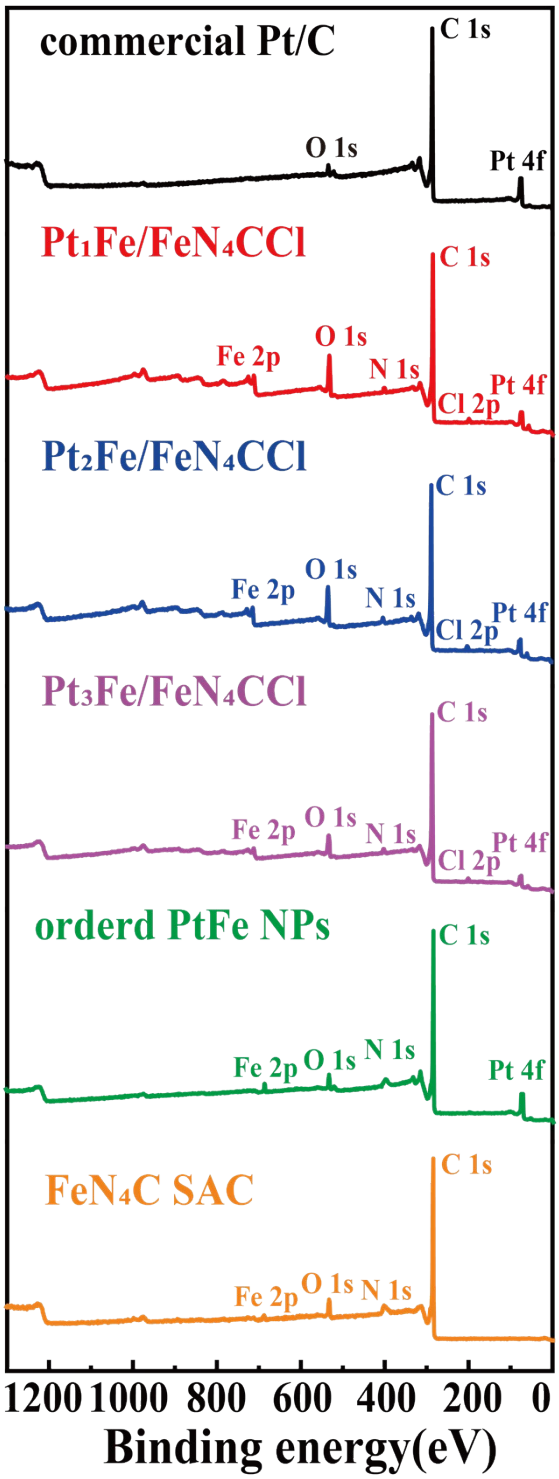

Figure S8 The XPS survey spectrum of commercial Pt/C, FeN_4C SAC, Pt_1Fe/FeN_4CCl, Pt_2Fe/FeN_4CCl, Pt_3Fe/FeN_4CCl, and ordered PtFe NPs catalyst.

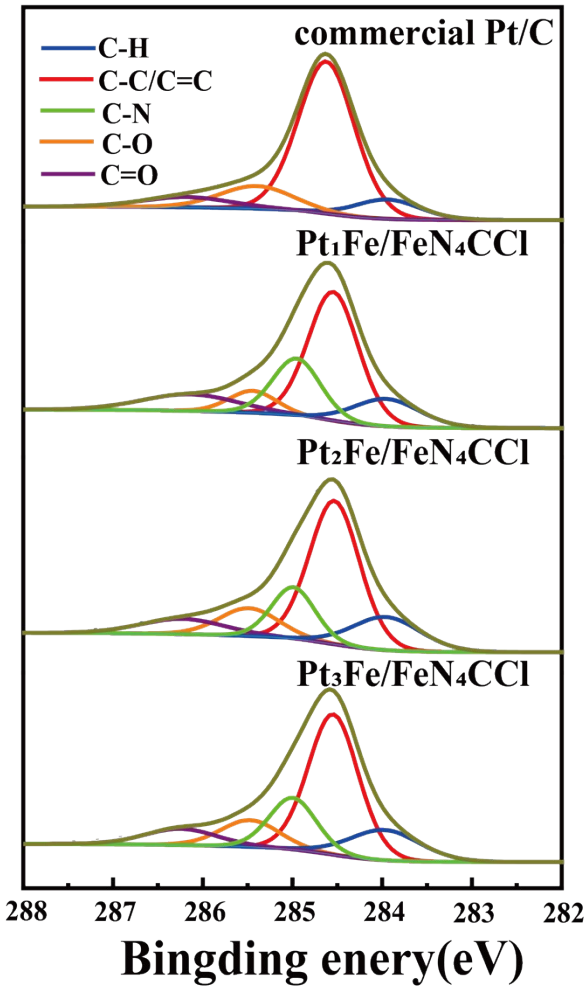

Figure S9 C 1s spectra of commercial Pt/C, Pt_1Fe/FeN_4CCl, Pt_2Fe/FeN_4CCl and Pt_3Fe/FeN_4CCl catalyst. It has a lower ratio of C-C/C=C than that of prepare catalyst, demonstrating that the side chain axial-coordinated Cl atoms lead to more distorted graphitic carbon species with high temperature pyrolysis. The fitted peak of C1s contains C-N peaks compared with commercial Pt/C catalyst, indicating presumable nitrogen-dope in the as-prepared catalyst support.

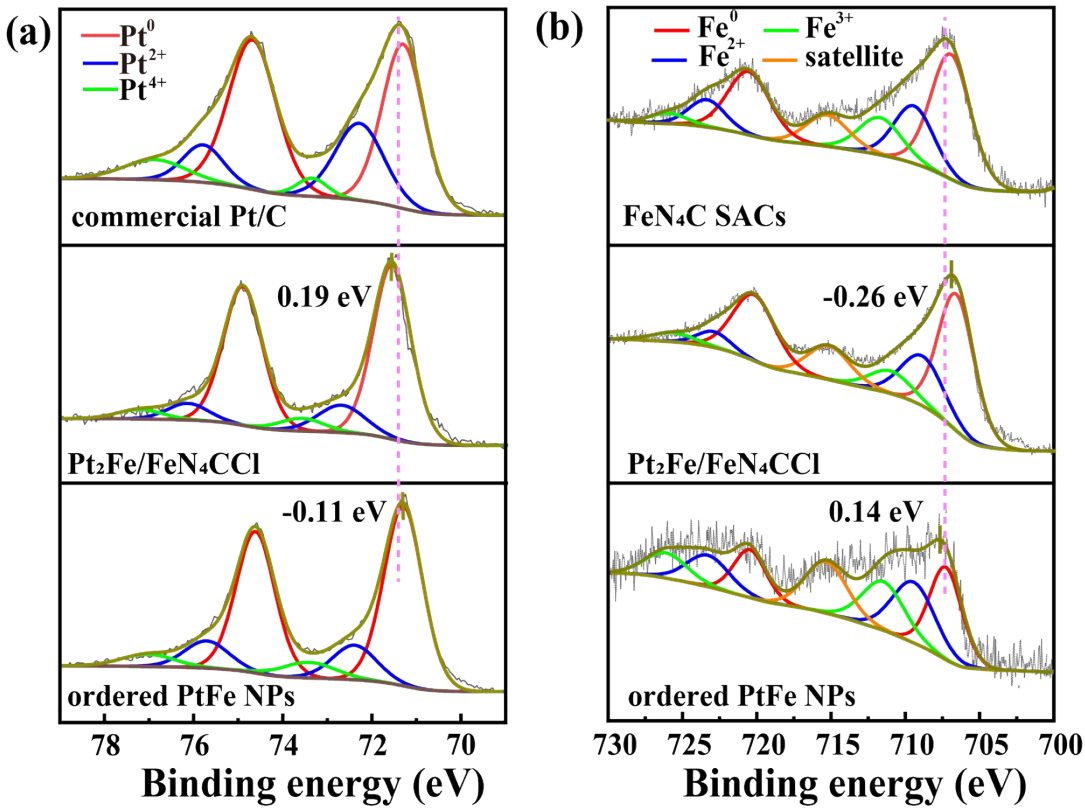

Figure S10 (a) Pt 4f spectra of commercial Pt/C, Pt_2Fe/FeN_4CCl and ordered PtFe NPs catalyst. (b) Fe 2p spectra of commercial FeN_4C, Pt_2Fe/FeN_4CCl and ordered PtFe NPs catalyst.

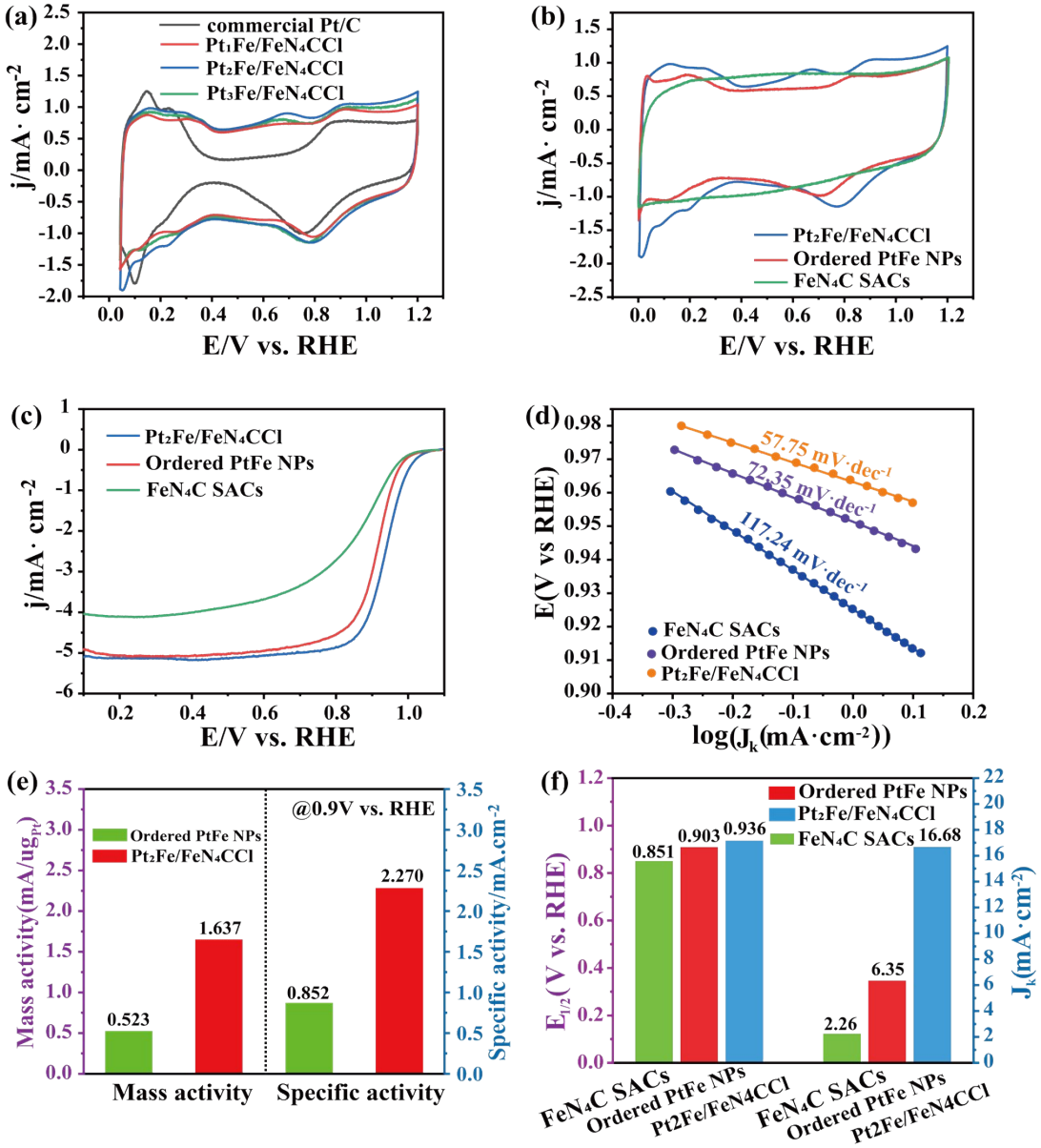

Figure S11 (a-b) CV curves of FeN_4C SACs, Pt_1Fe/FeN_4CCl, Pt_2Fe/FeN_4CCl, Pt_3Fe/FeN_4CCl, ordered PtFe NPs and commercial Pt/C. Testing condition: CV scan rate of 50 mV s^{-1}, N_2-saturated 0.1 M $HClO_4$ solution. (**c**)LSV curves of Pt_2Fe/FeN_4CCl, ordered PtFe NPs and FeN_4C SACs in O_2-saturated 0.1 M $HClO_4$ solution, sweep rate 10 mV/s, and rotation rate 1600 rpm. (**d**) the Tafel plots of Pt_2Fe/FeN_4CCl, ordered PtFe NPs and FeN_4C SACs. (**e**) the MA and SA of ordered PtFe NPs and Pt_2Fe/FeN_4CCl catalyst. (**f**) half-wave potential of the ORR driven by Pt_2Fe/FeN_4CCl, ordered PtFe NPs and FeN_4C SACs and the current density.

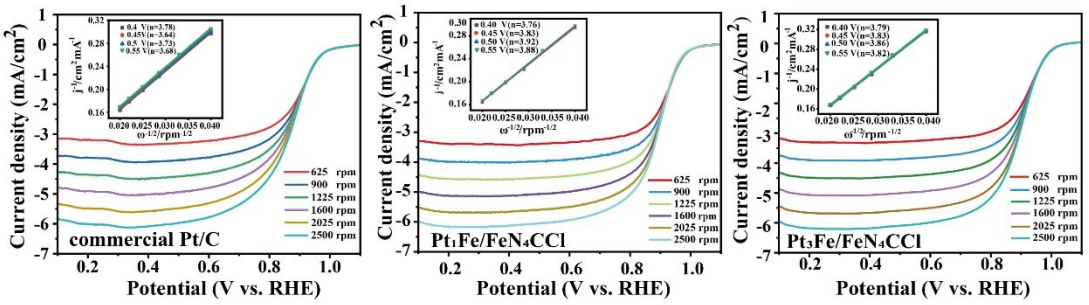

Figure S12 ORR polarization curves of commercial Pt/C, Pt_1Fe/FeN_4CCl and Pt_3Fe/FeN_4CCl catalysts at various rotation rates, and Koutecky-Levich plots at various electrode potentials(inset).

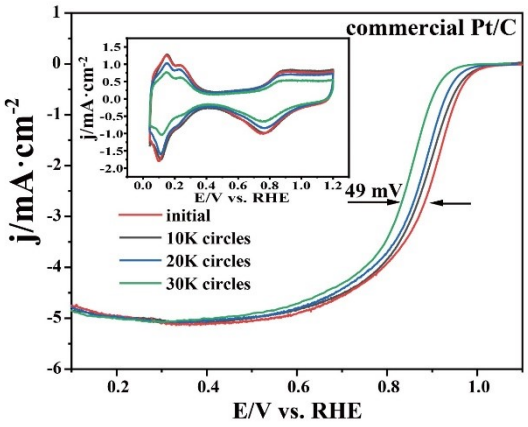

Figure S13 ORR polarization curves of commercial Pt/C catalysts at long-term operation durability (inset is the CV curves of commercial Pt/C catalysts). The accelerated durability test was carried out by applying10,000-30,000 CV cycles of potential sweeps between 0.6 and 1.1V VS. RHE in O_2-saturated 0.1 M $HClO_4$ at a scan rate of 50mV·s^{-1}.

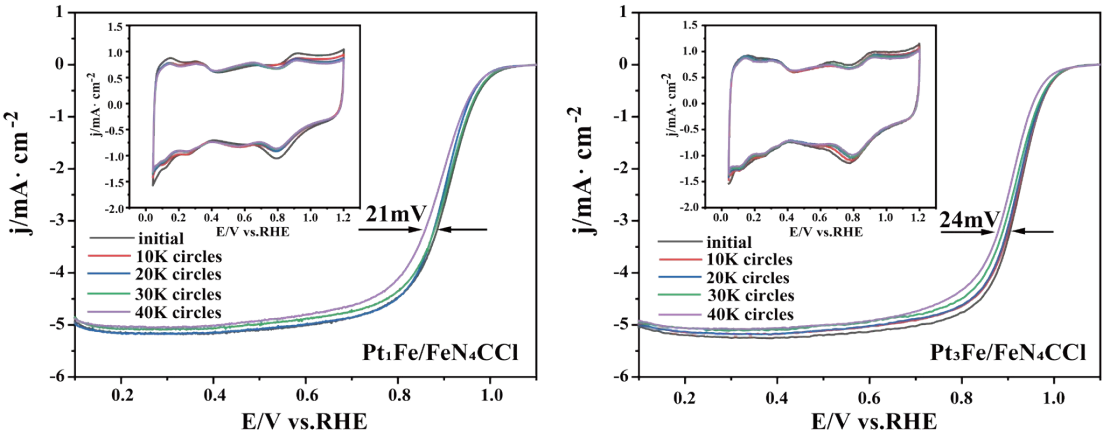

Figure S14 ORR polarization curves of Pt_1Fe/FeN_4CCl and Pt_3Fe/FeN_4CCl catalysts at long-term operation durability (inset is the CV curves). The accelerated durability test was carried out by applying10,000-40,000 CV cycles of potential sweeps between 0.6 and 1.1V VS. RHE in O_2-saturated 0.1 M $HClO_4$ at a scan rate of 50mV·s^{-1}.

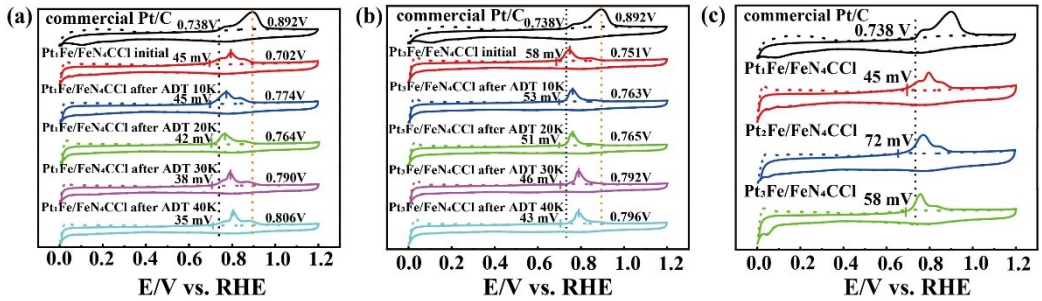

Figure S15 CO stripping voltammetry in 0.1 M $HClO_4$ electrolyte (scan rate:30 mV/s) of Pt_1Fe/FeN_4CCl, Pt_3Fe/FeN_4CCl and commercial Pt/C catalyst.

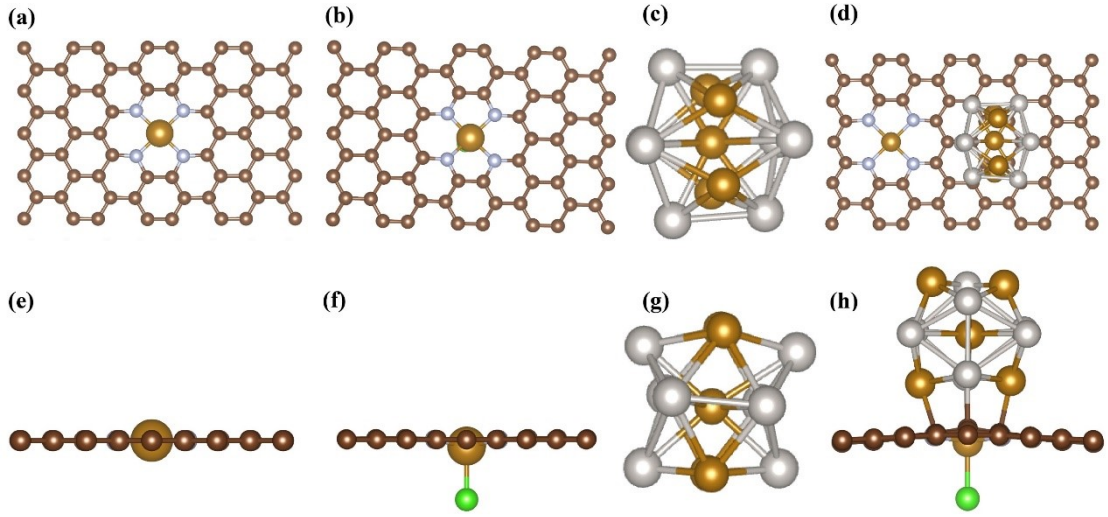

Figure S16 The constructed the structural model (top and side views) of (a, e) FeN_4C, (b, f) FeN_4Cl, (c, g) PtFe and (d, h) PtFe/ FeN_4CCl.

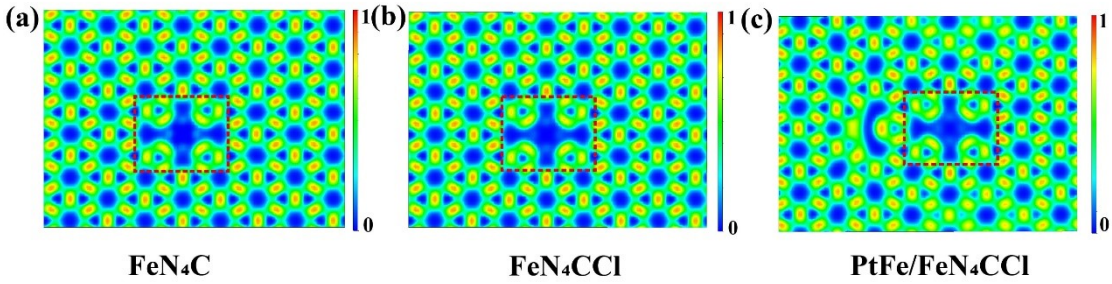

Figure S17 Electron localization functions of the center Fe site of (a) FeN_4C, (b) FeN_4CCl and (c) $PtFe/FeN_4CCl$. It proves that FeN_4C, FeN_4CCl and $PtFe/FeN_4CCl$ with FeN_4 configuration feature plane exhibits symmetrical electron localization distribution, which the orbital electron delocalization of Fe center in the crystal was induced by the axial-coordinated traction of Cl atoms.

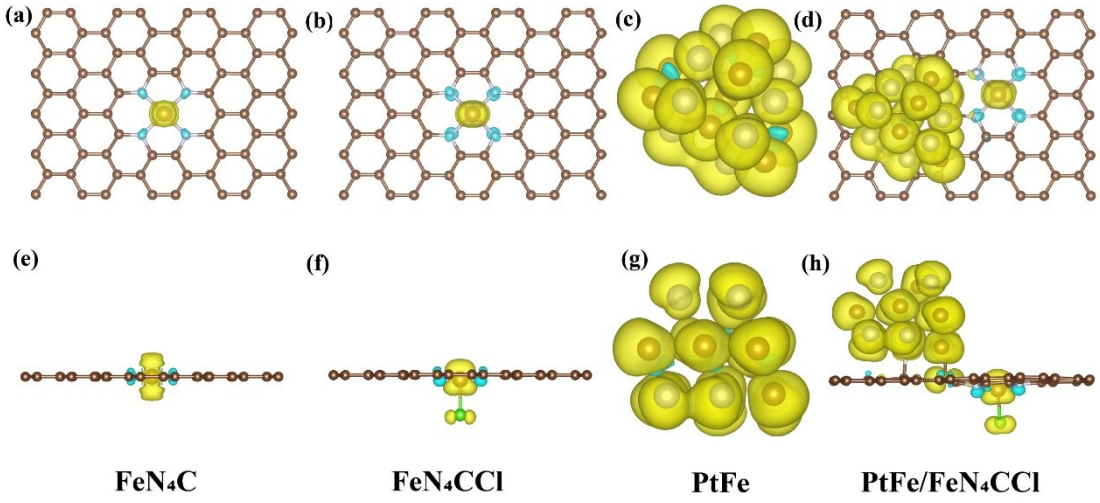

Figure S18 Top and side views of spin density distribution diagram for FeN_4C, FeN_4CCl, PtFe and PtFe/FeN_4CCl, respectively.

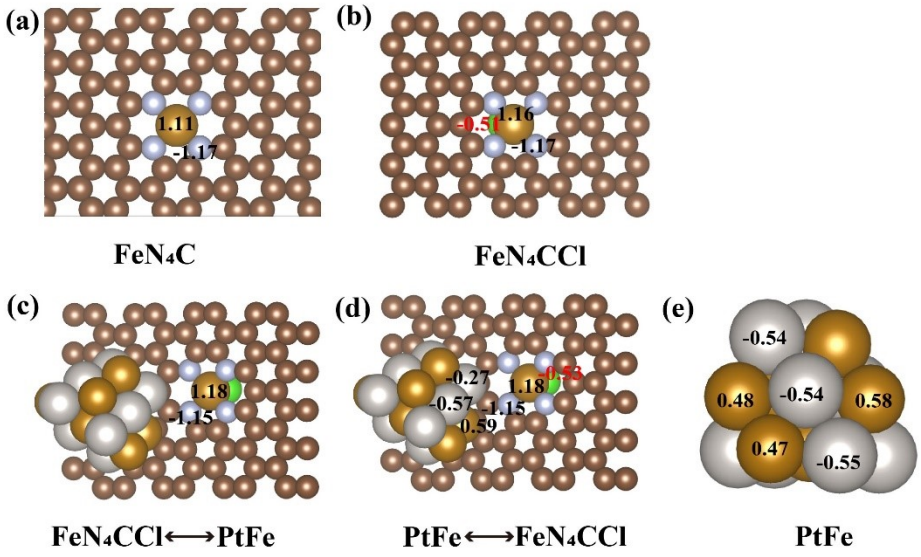

Figure S19 Top views of Bader charge distribution scheme for FeN_4C, FeN_4CCl, PtFe/FeN_4CCl, and PtFe, respectively.

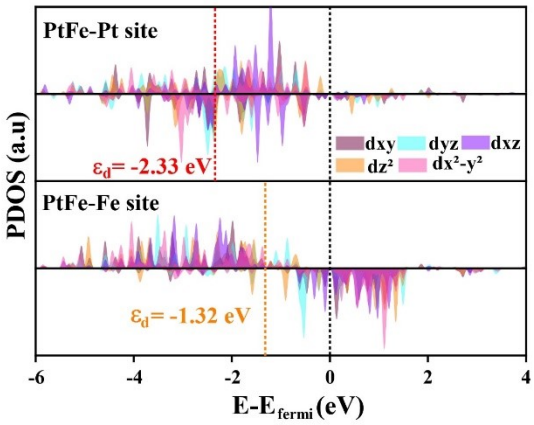

Figure S20 The density of states (DOS) diagram of PtFe the adsorption Metal site (Fe and Pt) with O_2 molecule.

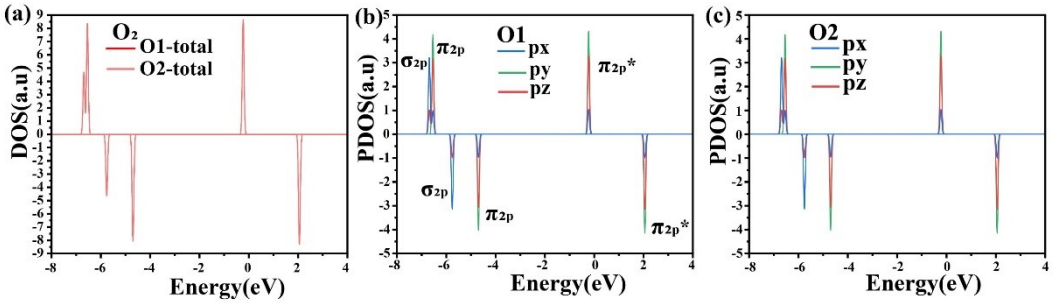

Figure S21 The density of states (DOS) diagram of O_2 molecule (a) and the partial density of states (PDOS) diagram of O1 (b) and O2 (c) atoms.

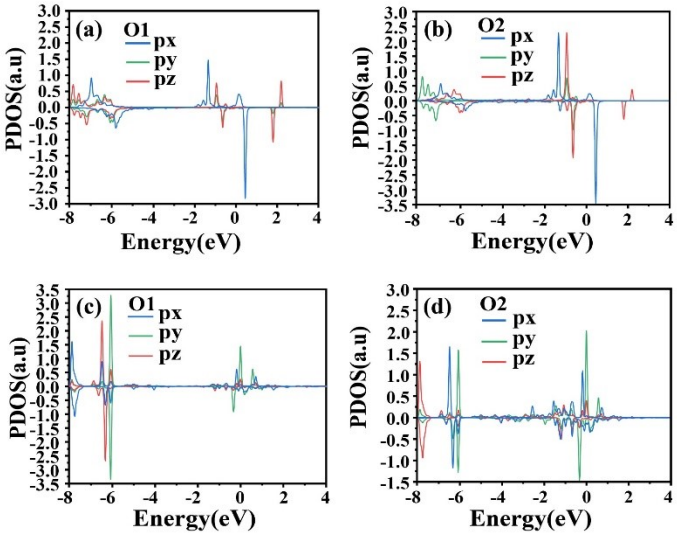

Figure S22 The partial density of states (PDOS) of O1 and O2 atoms diagram of the adsorption Fe site and Pt site based on PtFe/FeN_4CCl catalyst with O_2, which is show in (a-b) on Fe site and in (c-d) on Pt site.

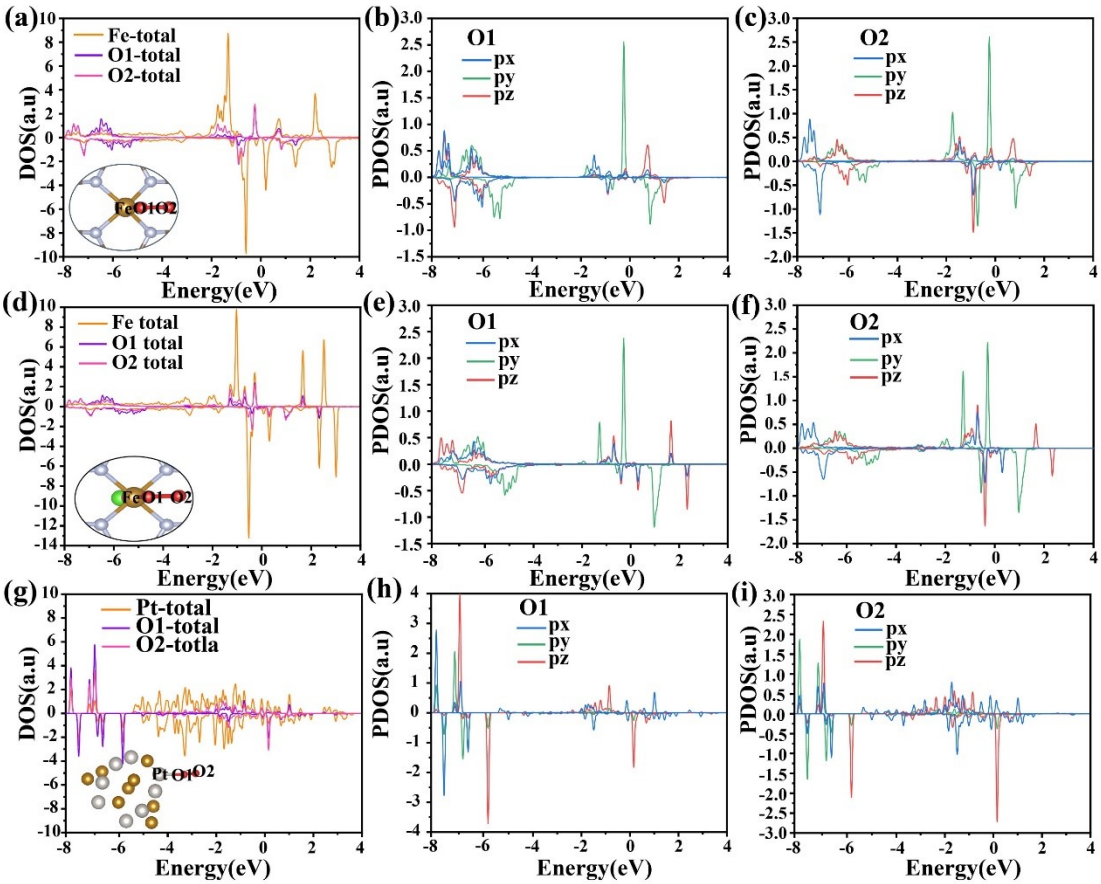

Figure S23 The density of states (DOS) diagram of the adsorption metal Fe and Pt site with O_2 molecule for FeN_4C (a), FeN_4CCl (d) , PtFe (g） and corresponding the partial density of states (PDOS) of O1 and O2 atoms in Fe site (b-c), (e-f), and (h-i). The inset is the model of Metal sites (Fe and Pt) and oxygen atoms for FeN_4C, FeN_4CCl, PtFe, respectively.

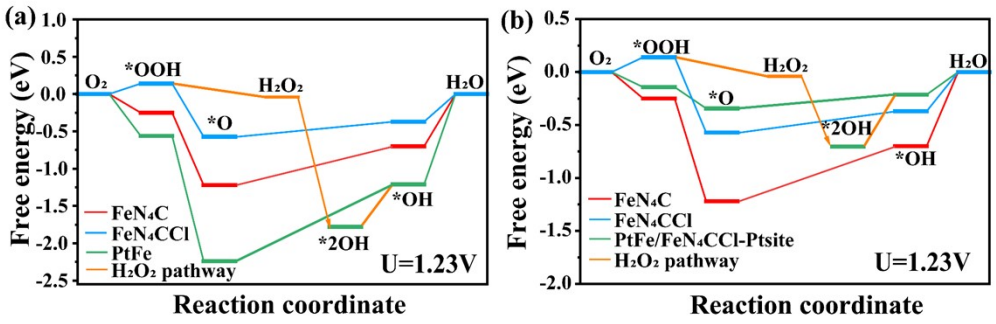

Figure S24 Free energy diagram of the ORR pathways for FeN_4C, FeN_4CCl and PtFe sites for DFT. Synergistic ORR catalytic pathways involved in H_2O_2 reaction mechanism over FeN_4C, FeN_4CCl and PtFe-Pt site.

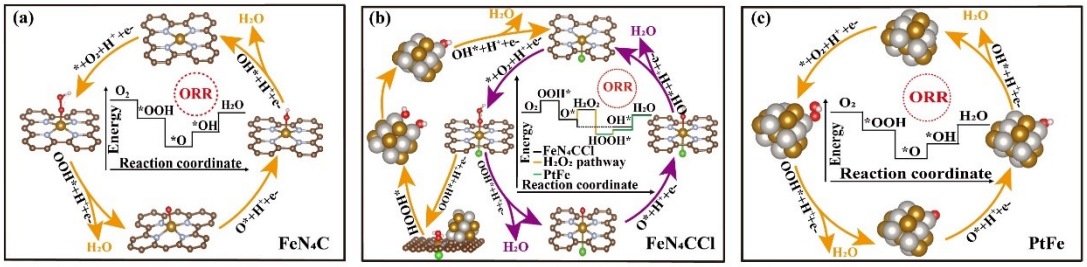

Figure S25 Scheme of the pathway in ORR mechanism of FeN_4C, FeN_4CCl, PtFe based on DFT, respectively. The H_2O_2 adsorbate at Fe sites can release and migrate to the contiguous Pt sites for successive 2e- reaction, thereby effectuating integral oxygen reduction.

Supplementary Tables

Table S1. The detailed ordered degree and alloy degree for Pt_1Fe/FeN_4CCl, Pt_2Fe/FeN_4CCl, and Pt_3Fe/FeN_4CCl as compared to the standard PDFs of PtFe (PDF#43-1359) from the XRD patterns, respectively.

Sample	I_{110}/I_{111}	I_{001}/I_{111}	Lattice Strain%
PtFe (PDF#43-1359)	0.280	0.300	N/A
Pt_1Fe/FeN_4CCl	0.233	0.294	2.81
Pt_2Fe/FeN_4CCl	0.275	0.391	3.13
Pt_3Fe/FeN_4CCl	0.266	0.338	2.99

Table S2 The elemental loadings of the as-prepared Pt_1Fe/FeN_4CCl, Pt_2Fe/FeN_4CCl and Pt_3Fe/FeN_4CCl catalysts by using ICP-OES.

catalyst	ICP (Before Stability test) Loading by weight % relative to the whole sample		ICP (Before Stability test) Loading by atomic % relative to the whole sample		ICP (After Stability test) Loading by weight % relative to the whole sample		ICP (After Stability test) Loading by atomic % relative to the whole sample	
	Pt	Fe	Pt	Fe	Pt	Fe	Pt	Fe
Pt_1Fe/FeN_4CCl	10.02	9.79	0.77	2.63	9.91	9.75	0.76	2.61
Pt_2Fe/FeN_4CCl	10.29	6.28	0.76	1.62	10.17	6.25	0.75	1.61
Pt_3Fe/FeN_4CCl	10.55	3.58	0.75	0.89	10.42	3.55	0.74	0.88

Table S3 Structural parameters of Pt foil, Pt_2Fe/FeN_4CCl, and PtO_2 extracted from the EXAFS fitting ($S0^2$= 0.76).

Sample	Path	CN	R(Å)	σ^2(Å^2)	ΔE0 (eV)	R factor
Pt foil	Pt-Pt	12*	2.77±0.010	0.0066±0.0008	11.9±0.9	0.012
Pt_2Fe/FeN_4CCl	Pt-Fe	4.14±0.36	2.62±0.013	0.0018±0.0017		
	Pt-Pt	6.25±1.65	2.73±0.025	0.0012±0.0025	9.08±3.09	0.017
	Pt-N	1.46±0.73	1.95±0.030	0.0043±0.0006		
PtO_2	Pt-O	5.26±0.54	2.02±0.012	0.0006±0.0012	5.92±1.85	0.027
	Pt-Pt	7.36±2.63	3.12±0.018	0.0085±0.0035	14.95±1.16	

Note: $S0^2$ is the amplitude reduction factor (obtained by the fitting of Pt foil); CN is the coordination number; R is interatomic distance (the bond length between Pt central atoms and surrounding coordination atoms); ΔE_0 is energy shift; σ^2 is Debye-Waller factor (a measure of thermal and static disorder in absorber-scatterer distances); R-factor is used to value the goodness of the fitting; * the experimental EXAFS fit of metal foil by fixing CN as the known crystallographic value.

Table S4 Structural parameters of Fe foil, FeO, FePc and Pt_2Fe/FeN_4CCl extracted from the EXAFS fitting ($S0^2$= 0.7).

Sample	Path	CN	R(Å)	σ^2(Å^2)	ΔE0 (eV)	R factor
Fe foil	Fe-Fe	6*	2.84±0.023	0.0050±0.0032	4.01±3.07	0.009
	Fe-Fe	8*	2.46±0.022	0.0054±0.0023		
FeO	Fe-Fe	12.46	3.07±0.029	0.0148±0.0019	0.85±0.67	0.004
	Fe-O	5.48	2.12±0.027	0.0129±0.0009		
FePC	Fe-N	4.28	1.93±0.014	0.0076±0.0024	2.35±0.08	0.015
	Fe-C	7.78	2.96±0.023	0.0049±0.0029		
Pt_2Fe/FeN_4CCl	Fe-Pt	8.08	2.78±0.024	0.0118±0.0258	7.58±1.88	0.015
	Fe-Fe	4.12	2.55±0.018	0.0105±0.0017		
	Fe-Cl	1.35	2.06±0.010	0.0040±0.0027		
	Fe-N	3.89	1.92±0.035	0.0040±0.0027		

Note: $S0^2$ is the amplitude reduction factor (obtained by the fitting of Fe foil); CN is the coordination number; R is interatomic distance (the bond length between Fe central atoms and surrounding coordination atoms); ΔE_0 is energy shift; σ^2 is Debye-Waller factor (a measure of thermal and static disorder in absorber-scatterer distances); R-factor is used to value the goodness of the fitting; * the experimental EXAFS fit of metal foil by fixing CN as the known crystallographic value.

Table S5 The percentages of atomic content for C 1s, Pt 4f, N 1s, O 1s, Fe 2p Cl 2p corresponding to the XPS survey spectrum

Catalysts	Name	C 1s	N 1s	O 1s	Pt 4f	Fe 2p	Cl 2p
Pt/C	Atomic%	97.49	N/A	0.98	1.53	N/A	N/A
	Weight %	78.84	N/A	1.06	20.10	N/A	N/A
FeN_4C SACs	Atomic%	91.04	5.14	1.25	N/A	2.57	N/A
	Weight %	82.28	5.42	1.50	N/A	10.80	N/A
Ordered PtFe NPs	Atomic%	92.05	5.31	1.05	0.76	0.83	N/A
	Weight %	79.46	5.35	1.21	10.66	3.33	N/A
Pt_1Fe/FeN_4CCl	Atomic%	86.53	7.38	1.07	0.77	2.64	1.61
	Weight %	68.51	6.83	1.13	10.02	9.74	3.77
Pt_2Fe/FeN_4CCl	Atomic%	92.35	3.35	1.14	0.76	1.62	0.78
	Weight %	76.98	3.26	1.27	10.29	6.28	1.92
Pt_3Fe/FeN_4CCl	Atomic%	96.40	0.62	1.15	0.75	0.90	0.19
	Weight %	83.44	0.63	1.33	10.55	3.58	0.49

Table S6 The C 1s XPS spectra binding energy and relative ratio of C-C,C-N，C=C，C-O and C=O of Pt_1Fe/FeN_4CCl, Pt_2Fe/FeN_4CCl, Pt_3Fe/FeN_4CCl and commercial Pt/C catalyst after separating peak.

Sample	C-H		C-C/C=C		C-N		C-O		C=O	
	Binding energy(eV)	Relative ratio (%)	Binding energy(eV)	Relative ratio (%)	Binding energy(eV)	Relative ratio (%)	Binding energy(eV)	Relative ratio (%)	Binding energy(eV)	Relative ratio (%)
Pt/C	284.62	70.27	283.93	10.24	N/A	N/A	285.39	13.62	286.18	5.88
Pt_1Fe/FeN_4CCl	284.52	49.29	283.94	15.47	284.98	15.29	285.47	11.27	286.22	8.68
Pt_2Fe/FeN_4CCl	284.54	47.40	283.95	13.31	284.95	20.07	285.44	11.58	286.14	7.64
Pt_3Fe/FeN_4CCl	284.54	49.12	283.97	14.88	284.99	17.00	285.47	10.88	286.24	8.12

Table S7 The percentages of Pyridinic-N (%), Pyrrolic-N (%), Graphitic-N (%), Fe-N_x (%) and Oxidized-N (%) N 1s corresponding to the XPS survey spectrum.

Sample	Pyridinic-N (%)		Fe-N_x (%)		Pyrrolic-N (%)		Graphitic- N (%)		Oxidized-N (%)	
	Binding energy(eV)	Relative ratio (%)	Binding energy(eV)	Relative ratio (%)	Binding energy(eV)	Relative ratio (%)	Binding energy(eV)	Relative ratio (%)	Binding energy(eV)	Relative ratio (%)
Pt_1Fe/FeN_4CCl	398.20	32.10	399.21	17.10	400.13	20.90	401.28	24.00	402.90	5.90
Pt_2Fe/FeN_4CCl	398.20	30.55	399.21	16.68	400.14	24.73	401.28	19.08	402.90	8.96
Pt_3Fe/FeN_4CCl	398.21	32.88	399.21	21.73	400.14	22.06	401.27	15.43	402.84	7.90

Table S8 The Pt 4f XPS spectra binding energy and relative ratio of Pt^0, Pt^{2+} and Pt^{4+} of Pt_1Fe/FeN_4CCl, Pt_2Fe/FeN_4CCl, Pt_3Fe/FeN_4CCl and commercial Pt/C catalyst after separating peak.

Sample	Pt^0		Pt^{2+}		Pt^{4+}	
	Binding energy(eV)	Relative ratio (%)	Binding energy(eV)	Relative ratio (%)	Binding energy(eV)	Relative ratio (%)
Pt/C	71.38 74.75	66.44	72.35 75.68	25.08	73.41 76.94	8.49
Ordered PtFe NPs	71.28 74.63	74.79	72.41 75.71	16.33	73.42 77.04	8.88
Pt_1Fe/FeN_4CCl	71.45 74.79	78.04	72.64 76.14	18.50	73.63 77.16	3.46
Pt_2Fe/FeN_4CCl	71.47 74.80	80.37	72.67 76.25	15.39	73.59 77.19	4.24
Pt_3Fe/FeN_4CCl	71.54 74.89	80.32	72.67 76.12	13.10	73.56 77.19	6.58

Table S9 The Fe 2p XPS spectra binding energy and relative ratio of Fe^0, Fe^{2+}, Fe^{3+} and Satellite of Pt_1Fe/FeN_4CCl, Pt_2Fe/FeN_4CCl, and Pt_3Fe/FeN_4CCl catalyst after separating peak.

Sample	Fe^0		Fe^{2+}		Fe^{3+}		Satellite	
	Binding energy(eV)	Relative ratio (%)	Binding energy(eV)	Relative ratio (%)	Binding energy(eV)	Relative ratio (%)	Binding energy(eV)	Relative ratio (%)
FeN_4C SACs	707.04 720.68	63.23	709.56 723.49	21.41	711.79 726.20	6.62	715.24	8.74
Ordered PtFe NPs	707.32 720.22	33.01	709.13 723.08	28.45	711.18 725.84	22.73	715.02	15.81
Pt_1Fe/FeN_4CCl	706.81 720.42	58.78	709.11 723.15	20.11	711.02 725.90	10.20	715.39	10.91
Pt_2Fe/FeN_4CCl	706.90 720.31	62.84	709.09 723.15	19.88	710.98 725.99	8.85	715.25	8.43
Pt_3Fe/FeN_4CCl	706.95 720.34	52.69	709.15 723.18	22.47	711.05 725.83	13.23	715.23	11.61

Table S10 The Cl 2p XPS spectra binding energy and relative ratio of Fe-Cl and Organic Cl of Pt_1Fe/FeN_4CCl, Pt_2Fe/FeN_4CCl, and Pt_3Fe/FeN_4CCl catalyst after separating peak.

Sample	Fe-Cl		Organic Cl	
	Binding energy(eV)	Relative ratio (%)	Binding energy(eV)	Relative ratio (%)
Pt_1Fe/FeN_4CCl	198.50 200.04	67.55	201.03 202.42	32.45
Pt_2Fe/FeN_4CCl	198.50 200.13	83.99	201.03 202.43	16.01
Pt_3Fe/FeN_4CCl	198.48 200.02	75.79	200.98 202.37	24.21

Table S11 Pt loading, $ECSA_{CO}$, half-wave potential, mass activity, specific activity at 0.9V, and ICP loading by weight of commercial Pt/C, FeN_4C SACs, Ordered PtFe NPs, Pt_1Fe/FeN_4CCl, Pt_2Fe/FeN_4CCl and Pt_3Fe/FeN_4CCl catalyst before ADT.

Sample	Pt loading (ug)	$ECSA_{CO}$ (m^2/g)	Halfwave potential (V)	Mass activity@0.9V (A/mg_{Pt})	Specific activity@0.9V (mA/cm^2)	Pt loading of catalyst (ICP)
Pt/C	4.00	62.26	0.876	0.165	0.264	20.10%
FeN_4C SACs	N/A	N/A	0.851	N/A	N/A	N/A
Ordered PtFe NPs	2.00	61.38	0.903	0.523	0.852	10.66%
Pt_1Fe/FeN_4CCl	2.00	67.38	0.909	0.605	0.899	10.02%
Pt_2Fe/FeN_4CCl	2.00	72.12	0.936	1.637	2.270	10.29%
Pt_3Fe/FeN_4CCl	2.00	69.53	0.920	0.738	1.061	10.55%

Table S12 Pt loading, $ECSA_{CO}$, half-wave potential, mass activity, specific activity at 0.9V, and ICP loading by weight of commercial Pt/C, Pt_1Fe/FeN_4CCl, Pt_2Fe/FeN_4CC and Pt_3Fe/FeN_4CCl catalyst after ADT.

Sample	Pt loading (ug)	$ECSA_{CO}$ (m^2/g)	Halfwave potential (V)	Mass activity@0.9V (A/mg_{Pt})	Specific activity@0.9V (mA/cm^2)	Pt loading of catalyst (ICP)
Pt/C	4.00	91.07	0.827	0.102	0.112	19.86%
Pt_1Fe/FeN_4CCl	2.00	69.51	0.885	0.529	0.761	9.81%
Pt_2Fe/FeN_4CCl	2.00	72.89	0.920	1.509	2.070	10.17%
Pt_3Fe/FeN_4CCl	2.00	70.69	0.899	0.608	0.856	10.42%

Table S13 Comparisons of the ORR performance in recently published papers.

Catalysts	MA (A/mg_{Pt})	SA (mA/cm^2)	Electrolytes	References
Pt1Fe1-IMC/C	0.45	0.99	0.1 M $HClO_4$	5
PtFe-H/Pt	0.92	1.31	0.1 M $HClO_4$	6
PtA@FeSA–N–C	0.86	1.21	0.1 M $HClO_4$	7
$L1_2$-$Pt_3Fe/C_{Fe\text{-}N\text{-}C}$	1.010	1.166	0.1 M $HClO_4$	8
H-PtCo@Pt_1N-C	1.2	2.39	0.1 M $HClO_4$	9
PtCo/NGC	0.45	0.61	0.1 M $HClO_4$	10
Pt@Fe–N–OMC-2	0.53	0.97	0.1 M $HClO_4$	11
Pt_2Fe/FeN_4CCl	**1.637**	**2.270**	**0.1 M $HClO_4$**	**This work**

Table S14. The calculated magnetic moment of atom in FeN_4C, FeN_4CCl, PtFe and $PtFe/FeN_4CCl$ models.

Models	Fe	Cl	Pt
FeN_4C	1.91	N/A	N/A
FeN_4CCl	1.28	0.06	N/A
PtFe	3.21	N/A	0.42
$PtFe/FeN_4CCl$	1.49	0.08	0.35

Supplementary References

1 Ravel, B.; Newville, M., ATHENA, ARTEMIS, HEPHAESTUS: data analysis for X-ray absorption spectroscopy using IFEFFIT. *J. Synchrotron Radiat.* **2005**, 12 (4), 537-541.

2 Kresse, G.; Furthmüller, J., Efficient iterative schemes for ab initio total-energy calculations using a plane-wave basis set. *Phys. Rev. B* **1996**, 54 (16), 11169-11186.

3 Blöchl, P. E., Projector augmented-wave method. Phys. Rev. B 1994, 50 (24), 17953-17979.

4 Perdew, J. P.; Burke, K.; Ernzerhof, M., Generalized Gradient Approximation Made Simple. *Phys. Rev. Lett.* **1996**, 77 (18), 3865-3868.

5 Lai, D.; Cheng, Q.; Zheng, Y.; Zhao, H.; Chen, Y.; Hu, W.; Zou, Z.; Wen, K.; Zou, L.; Yang, H., A heteronuclear bimetallic organic molecule enabling targeted synthesis of an efficient Pt_1Fe_1 intermetallic compound for oxygen reduction reaction. *J. Mater. Chem. A* **2022**, 10 (31), 16639-16645.

6 Song, T. W.; Chen, M. X.; Yin, P.; Tong, L.; Zuo, M.; Chu, S. Q.; Chen, P.; Liang, H. W., Intermetallic PtFe Electrocatalysts for the Oxygen Reduction Reaction: Ordering Degree-Dependent Performance. *Small* **2022**, 18 (31), 2202916.

7 Ao, X.; Zhang, W.; Zhao, B.; Ding, Y.; Nam, G.; Soule, L.; Abdelhafiz, A.; Wang, C.; Liu, M., Atomically dispersed Fe–N–C decorated with Pt-alloy core–shell nanoparticles for improved activity and durability towards oxygen reduction. *Energy Environ. Sci.* **2020**, 13 (9), 3032-3040.

8 Jin, H.; Xu, Z.; Hu, Z.-Y.; Yin, Z.; Wang, Z.; Deng, Z.; Wei, P.; Feng, S.; Dong, S.; Liu, J.; Luo, S.; Qiu, Z.; Zhou, L.; Mai, L.; Su, B.-L.; Zhao, D.; Liu, Y., Mesoporous Pt@Pt-skin Pt_3Ni core-shell framework nanowire electrocatalyst for efficient oxygen reduction. *Nat. Commun.* **2023**, 14 (1), 107824.

9 Lai, W. H.; Zhang, B. W.; Hu, Z.; Qu, X. M.; Jiang, Y. X.; Wang, Y. X.; Wang, J. Z.; Liu, H. K.; Chou, S. L., The Quasi-Pt-Allotrope Catalyst: Hollow PtCo@single-Atom Pt1 on Nitrogen-Doped Carbon toward Superior Oxygen Reduction. *Adv. Funct. Mater.* **2019**, 29 (13), 1807340.

10 Jung, W. S.; Lee, W. H.; Oh, H.-S.; Popov, B. N., Highly stable and ordered intermetallic PtCo alloy catalyst supported on graphitized carbon containing Co@CN for oxygen reduction reaction. *J. Mater. Chem. A* **2020**, 8 (38), 19833-19842.

11 Wang, K.; Yang, H.; Wang, Q.; Yu, J.; He, Y.; Wang, Y.; Song, S.; Wang, Y., Electronic Enhancement Engineering by Atomic Fe–N_4 Sites for Highly-Efficient PEMFCs: Tailored Electric-Thermal Field on Pt Surface. *Adv. Energy Mater.* **2023**, 13 (14), 2204371.